J. Fluid Mech. (2007), *vol.* 570, *pp.* 455–466.
doi:10.1017/S0022112006002692 Printed in the United Kingdom

Motion of large bubbles in curved channels

By METIN MURADOGLU[1] AND HOWARD A. STONE[2]

[1]Department of Mechanical Engineering, Koc University, Rumelifeneri Yolu, Sariyer 34450 Istanbul, Turkey
mmuradoglu@ku.edu.tr

[2]Division of Engineering and Applied Sciences, Harvard University, Cambridge, MA 02138, USA
has@deas.harvard.edu

(Received 3 November 2005 and in revised form 17 July 2006)

We study the motion of large bubbles in curved channels both semi-analytically using the lubrication approximation and computationally using a finite-volume/front-tracking method. The steady film thickness is governed by the classical Landau–Levich–Derjaguin–Bretherton (LLDB) equation in the low-capillary-number limit but with the boundary conditions modified to account for the channel curvature. The lubrication results show that the film is thinner on the inside of a bend than on the outside of a bend. They also indicate that the bubble velocity relative to the average liquid velocity is always larger in a curved channel than that in a corresponding straight channel and increases monotonically with increasing channel curvature. Numerical computations are performed for two-dimensional cases and the computational results are found to be in a good agreement with the lubrication theory for small capillary numbers and small or moderate channel curvatures. For moderate capillary numbers the numerical results for the film thickness, when rescaled to account for channel curvature as suggested in the lubrication calculation, essentially collapse onto the corresponding results for a bubble in a straight tube. The lubrication theory is also extended to the motion of large bubbles in a curved channel of circular cross-section.

1. Introduction

The research and development of microfluidic methods as part of a toolbox for rapid chemical analysis, synthesis, screening and other lab-on-a-chip scenarios has inspired new ideas in multiphase flow, mixing, and other transport processes that involve fluid dynamics (e.g. Squires & Quake 2005; Stone, Stroock & Ajdari 2004). Here we draw inspiration from one recent set of experimental studies focused on using a sequence of injected gas bubbles in a flow in a curved channel as a means to affect mixing of the continuous liquid phase (Guenther *et al.* 2004, 2005; Garstecki, Fischbach & Whitesides 2005). Typically, the gas bubbles have a length greater than the channel width and are separated from the channel walls by thin films of the wetting, continuous-phase liquid. The film thickness profile is important for characterizing the 'leakage' of the continuous phase past the bubble. For small and moderate capillary numbers characteristic of the experiments, we show using numerical simulations that the film is thinner on the inside of a bend than the outside of a bend. Using a lubrication approach we then map this problem to the well-known Landau–Levich–Derjaguin–Bretherton (LLDB) problem (Quere 1999; Landau & Levich 1942; Bretherton 1961), and so arrive at an analytical description

valid for the small-capillary-number limit, which is in good agreement with the numerical simulations.

In the experiments of Guenther *et al.* (2004, 2005) (see also Garstecki *et al.* 2005) gas bubbles are periodically injected into a steady liquid flow. Relative to the bubbles, the continuous-phase fluid between the bubbles is forced to circulate and advectively enhanced mixing, or stirring, of the fluid is triggered by using a wavy channel centreline. The gas bubbles are then removed downstream after mixing is accomplished. This 'segmented' gas–liquid flow was shown to be more effective in reducing the length of the channel necessary to achieve a given degree of mixing than other micromixing approaches. In addition, the authors suggested that this approach to mixing can be operated with a wide range of flow rates, which allows it to be used for chemical reactors with both slow and fast kinetics. A quantitative characterization of the different aspects of the fluid dynamics, mixing, and dispersion of this type of flow requires consideration of the flow at the scale of a single bubble. In particular, the leakage flow from one bubble to the next bubble upstream requires understanding the flow through the thin films around the bubble. For an example of the analogous idea of a wavy channel applied to enhance mixing inside drops, see the original experiments of Song *et al.* (2003), and numerical models of Stone & Stone (2005) and Muradoglu & Stone (2005).

As is well known, when a long bubble translates in a straight channel the continuous-phase liquid leaks through the thin films (Bretherton 1961); the case of a bubble in a rectangular cross-section channel has also been studied (e.g. Wong, Radke & Morris 1995 and Thulasidas, Abraham & Cerro 1995). In a straight circular tube the bubble speed U_b is larger than the average speed of the continuous-phase liquid U_c, with the difference in speeds controlled by the capillary number, $Ca = \mu U_b/\sigma$, which sets the mean film thickness; in particular, Bretherton has shown $U_b - U_c = 2c_1 U_b Ca^{2/3}$ where the constant $c_1 = 1.3375$.

In this paper we consider the analogous problem for a bubble in a wavy channel. Related low-Reynolds-number studies, involving both boundary-element numerical simulations and the lubrication approximation, include Gaver *et al.* (1996), who studied a semi-infinite bubble moving through a flexible-walled channel as a model for re-opening of pulmonary airways, and Halpern & Jensen (2002), who characterized the motion of a semi-infinite bubble into a uniformly convergent channel. These types of problems are similar to other studies of thin films on curved substrates. For example, Schwartz & Weidner (1995) studied thin-film flows over an exterior corner and showed that the surface curvature is equivalent to a time-independent pressure distribution. Also, Roy, Roberts & Simpson (2002) developed a higher-order lubrication model for thin-film flows over curved surfaces to accurately include the effects of the substrate curvature, gravity and inertia. Reinelt (1995) studied the instability problem in a fluid that partially fills the gap between two off-centred rotating cylinders and pointed out the different film thicknesses of the inner and outer layers due to different wall velocities on the inner and outer cylinders but ignored the channel curvature effects. Thin-film flows driven by pressure gradients or body forces over a non-uniform topography were considered by Mazouchi & Homsy (2001), while Howell (2003) extended the lubrication models to include three-dimensional effects and a general characterization of the influence of the shape of the substrate. In this paper, we show that in the 'Bretherton', or low-capillary-number, limit the steady film thickness about a bubble translating in a channel or tube of constant centreline radius is governed by the classical LLDB equation but the boundary conditions are altered to account for the effects of the channel curvature. The lubrication model shows that the waviness

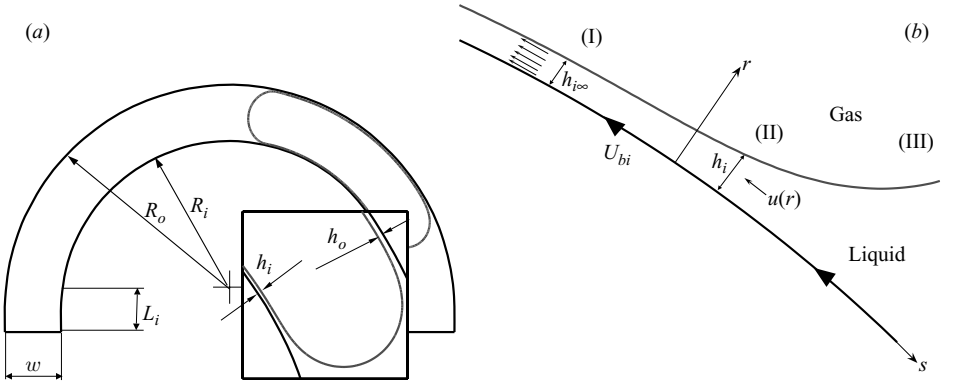

FIGURE 1. (*a*) Definition sketch for a large bubble moving through a circular channel, and (*b*) the curvilinear coordinate system (r, s) defined for the inner layer.

breaks the symmetry of the thin films on either side of the bubble, with the inside film being thinner than the outside film. The resulting film thickness can be expressed in the usual form as $h_\infty = c_1 \ell Ca_{\text{eff}}^{2/3}$ where ℓ and Ca_{eff} are, respectively, a properly defined length scale and an effective capillary number. The bubble velocity relative to the average liquid speed is then derived from mass conservation. Extensive numerical simulations are performed and the results are compared with the lubrication theory for small and moderate capillary numbers.

In § 2 we develop a lubrication model for the two-dimensional problem. A comparison of the numerical simulations and the lubrication predictions is given in § 3. The extension of these ideas for bubble motion in a curved channel of circular cross-section is given in § 4. Brief concluding remarks are given in § 5.

2. Bubble in a curved two-dimensional channel: a lubrication model

We consider a large gas bubble, with length much larger than the channel width w, moving steadily at velocity U_b in a two-dimensional circular channel as sketched in figure 1(*a*). The inner and outer radii of the channel are R_i and R_o, respectively. The flow rate in the channel is kept constant at $Q = U_c w$ where U_c is the average liquid velocity. Also, the ambient fluid, which is assumed to fully wet the channel, has density ρ and viscosity μ, and the surface tension is denoted by σ. Gravitational buoyancy effects and the dynamics of motion inside the bubble are neglected. For these conditions, the flow is characterized by a Reynolds number $Re = \rho U_c w/\mu$ and the capillary number $Ca = \mu U_b/\sigma$. It is further assumed that the capillary number is small, $Ca \ll 1$, and the Reynolds number is not too large, i.e. for the lubrication description given below $Re\, Ca \ll 1$, which follows from a comparison of the inertial and viscous terms, so that the inertial forces are also negligible compared to the viscous forces.

As the bubble moves in the channel, liquid films form between the bubble and the channel walls. The film thicknesses are denoted h_i and h_o for the inner and the outer layers, respectively. In the low-capillary-number limit, film thicknesses are much smaller than the channel width and the curvature of the interface varies slowly so that the 'lubrication' approximation is applicable in these thin-film regions (Bretherton 1961). We use a bubble-fixed plane polar coordinate system $(\mathscr{R}, \Theta)$ with the origin at the centre of the channel and Θ is measured in the clockwise direction. We also

define a local curvilinear coordinate system with the origin at (R_i, Θ_o), where Θ_o is an arbitrary constant angle. The curvilinear coordinate system is related to the polar coordinate system as $(r, s) = (\mathscr{R} - R_i, R_i\theta)$, where $\theta = \Theta - \Theta_o$ and $r = 0$ is the inner boundary (see figure 1*b*). The coordinate system rotates in the clockwise direction at the rate $\Omega = U_b/(R_i + w/2)$ as the bubble moves at constant velocity U_b in the channel. Therefore, the boundary conditions for a steady flow are no slip at the walls, i.e. $u_\theta(0, \theta) = -U_{b_i}$ and $u_\theta(w, \theta) = -U_{b_o}$ where $U_{b_i} = (2/(2+\beta))U_b$ and $U_{b_o} = (2 + 2\beta/2 + \beta)U_b$ with $\beta = w/R_i$, and no shear at the interface, i.e. $(\partial u_\theta/\partial r)(h_i, \theta) = (\partial u_\theta/\partial r)(w - h_o, \theta) = 0$. The shapes of the inner and outer layers $h_i(\theta)$ and $h_o(\theta)$ are to be determined. We first consider the inner layer and then generalize the results for the outer layer.

The application of the lubrication ideas to this configuration is standard. As sketched in figure 1(*b*), the inner layer consists of a semi-circular cap (region III), a circular film following the channel shape with a constant thickness $h_{i\infty}$ (region I), and a short intervening transition region (region II) where the curvature changes rapidly and dynamical effects are important. Using the usual lubrication approximations, the velocity profile in the inner film is given by

$$u_\theta = \frac{1}{2\mu}\frac{1}{R_i}\frac{\partial p}{\partial \theta}(r^2 - 2rh_i) - U_{b_i}. \tag{2.1}$$

Since the film thickness in region I is constant, mass conservation requires

$$U_{b_i}(h_i - h_{i\infty}) = -\frac{1}{3\mu}\frac{h_i^3}{R_i}\frac{\partial p}{\partial \theta}. \tag{2.2}$$

Furthermore, again within the lubrication approximation, the force balance in the normal direction at the interface dictates

$$p = p_g - \sigma\kappa, \tag{2.3}$$

where p_g is the constant pressure inside the bubble and κ is the curvature of the interface for two-dimensional flows and twice the mean curvature for three-dimensional flows. The curvature is given by

$$\kappa = -\frac{(R_i + h_i - h''_i)(R_i + h_i) + 2h_i'^2\cos 2\theta}{\left((R_i + h_i)^2 + h_i'^2\right)^{3/2}}, \tag{2.4}$$

where the prime denotes a derivative with respect to θ. Using the assumptions that the film thickness and the interface slope are small, i.e. $h_i/R_i \ll 1$ and $h'_i/R_i \ll 1$, equation (2.4) simplifies to

$$\kappa \cong -\frac{1}{R_i} + \frac{h''_i}{R_i^2}. \tag{2.5}$$

From equations (2.2), (2.3) and (2.5), we then obtain

$$h_i - h_{i\infty} = \frac{h_i^3}{3R_i^3 Ca_i}h'''_i, \tag{2.6}$$

where, in order to account for the geometry of the curved channel, the 'effective' capillary number Ca_i is defined as

$$Ca_i = \frac{\mu U_{b_i}}{\sigma} = \frac{2}{2+\beta}Ca. \tag{2.7}$$

The boundary conditions require that $h_i \to h_{i\infty}$, $h'_i \to 0$, $h''_i \to 0$ in region I and, using (2.5) and the fact that $\kappa \approx 2/w$ at the static circular cap, $h''_i \to 2R_i^2/w + R_i$ in region III (see figure 1*b*). The explicit dependence on the effective capillary number may be removed by the following non-dimensionalization and scaling:

$$\eta = \frac{h_i}{h_{i\infty}}, \quad \xi = \frac{R_i\theta}{h_{i\infty}}(3Ca_i)^{1/3}, \tag{2.8}$$

which yields the classical Landau–Levich equation

$$\frac{\mathrm{d}^3\eta}{\mathrm{d}\xi^3} = \frac{\eta - 1}{\eta^3}. \tag{2.9}$$

The boundary conditions are given in the usual form as $\eta \to 1$, $\eta' \to 0$, $\eta'' \to 0$ as $\xi \to -\infty$, and $\eta'' \to \alpha$ as $\xi \to \infty$, where $\alpha = 0.643$ is determined by numerical integration, as the problem is now in the familiar 'Bretherton' form. Then from equations (2.5) and (2.8), we obtain

$$h_{i\infty} = 1.3375 R_{\mathrm{eff}_i} Ca_i^{2/3}, \tag{2.10}$$

where the effective radius is defined as

$$R_{\mathrm{eff}_i} = \frac{wR_i}{2R_i + w} = \frac{1}{2+\beta}w. \tag{2.11}$$

Similarly, the film thickness in the outer layer can be found as

$$h_{o\infty} = 1.3375 R_{\mathrm{eff}_o} Ca_o^{2/3}, \tag{2.12}$$

where the effective radius and the capillary number are defined as

$$R_{\mathrm{eff}_o} = \frac{wR_o}{2R_o - w} = \frac{1+\beta}{2+\beta}w, \quad Ca_o = \mu\frac{U_{b_o}}{\sigma} = \frac{2+2\beta}{2+\beta}Ca. \tag{2.13}$$

It is clearly seen from equations (2.10) and (2.12) that the film thickness in the outer layer is always larger than that of the inner layer, which may have been anticipated since the relative velocity is higher for the outer film. To better see the effects of the channel curvature on the film thickness compared to the classical Bretherton solution, the film thicknesses scaled by the channel width can be re-written as

$$\frac{h_{i\infty}}{w} = \frac{1}{2+\beta}\left(\frac{2}{2+\beta}\right)^{2/3}\left(1.3375Ca^{2/3}\right), \tag{2.14}$$

$$\frac{h_{o\infty}}{w} = \frac{1+\beta}{2+\beta}\left(\frac{2+2\beta}{2+\beta}\right)^{2/3}\left(1.3375Ca^{2/3}\right), \tag{2.15}$$

so that the ratio of film thicknesses is

$$\frac{h_{o\infty}}{h_{i\infty}} = (1+\beta)^{5/3}. \tag{2.16}$$

Finally, using conservation of mass, the bubble speed relative to the average flow velocity in the channel is given by

$$\frac{U_b - U_c}{U_b} = 1.3375\left[\frac{2^{5/3}\left(1 + (1+\beta)^{8/3}\right)}{(2+\beta)^{8/3}}\right]Ca^{2/3}. \tag{2.17}$$

This result (take $\beta > 0$) shows that the bubble moves faster in a curved channel than in a corresponding straight channel for a specified constant flow rate; the asymmetry of the thicknesses of the thin films is the origin for this higher speed.

3. Results and discussion

Numerical simulations are performed for two-dimensional cases using a finite-volume (FV), front-tracking (FT) method developed by Muradoglu & Kayaalp (2006) and the computational results are compared with the lubrication theory. The front-tracking method is based on a single-field formulation of the flow equations for the entire computational domain and so treats different phases as a single Newtonian fluid with variable material properties (Unverdi & Tryggvason 1992). In this method, the interface between the bubble and the ambient fluid is represented by connected Lagrangian marker points moving with the local flow velocity interpolated from the neighbouring curvilinear grid points. The communication between the curvilinear grid and the marker points is maintained efficiently using the auxiliary grid method (Muradoglu & Kayaalp 2006). An indicator function is defined such that it is unity inside the bubble and zero outside. The indicator function is computed by solving a separable Poisson equation as described by Tryggvason *et al.* (2001) and is used to set fluid properties inside and outside the bubble. The marker points are also used to compute the surface tension forces at the interface and these forces are then distributed on the neighbouring curvilinear grid cells in a conservative manner. The surface tension forces are treated as body forces and added to the momentum equations as δ functions at the phase boundaries so that the flow equations can be solved using a conventional finite-volume method. The finite-volume method employed here is based on the concept of pseudo-time stepping and is second-order accurate both in time and space. The details of the front-tracking method can be found in Unverdi & Tryggvason (1992) and Tryggvason *et al.* (2001), and the version used in the present study is discussed in Muradoglu & Gokaltun (2004) and Muradoglu & Kayaalp (2006).

A typical computational domain is sketched in figure 1(*a*). The channel consists of a straight entrance section of length L_i, a circular main section with inner and outer radii of R_i and R_o, respectively, and a straight exit section of length $L_e = L_i$. The entrance and exit sections are added for convenience to implement the boundary conditions. A portion of a typical (coarse) curvilinear grid containing 220×22 cells is plotted as an inset in figure 2(*a*) to show the overall structure of the mesh used in the computations. The bubble velocity is computed indirectly, i.e. first the angular velocity of the bubble (Ω) is computed based on the velocity of the centre of the mass of the bubble and then the velocity of the bubble is computed as $U_b = (R_i + w/2)\Omega$. The grids are stretched near the solid walls to better resolve the thin films. Note that more grid points are used in the inner portion of the channel than the outer portion since the film thickness is expected to be thinner near the inner wall. In the cases of very low capillary numbers, i.e. $Ca \leqslant 0.01$, finer grids are used to avoid excessive grid stretching especially near the inner wall. An extensive grid convergence analysis was performed and the maximum numerical error in film thickness is kept below 5% in all the results presented in this paper. Both density and viscosity ratios are kept constant at 0.1 in all the results presented here. Although not shown here due to space limitations, an extensive study has been performed and shown that the effects of the viscosity ratio are negligible when $\lambda = \mu_{in}/\mu_{out} \leqslant 0.1$. Bubbles are initialized assuming hydrostatic conditions in a quiescent flow near the inlet section and then the flow is started instantaneously by imposing a constant flow rate at the inlet and keeping the pressure constant at the exit. Also, channel lengths are made sufficiently large so that the bubbles reach their steady shapes before exiting the channel. All computations are performed with a low value of the Reynolds number, i.e. $Re = 0.8$,

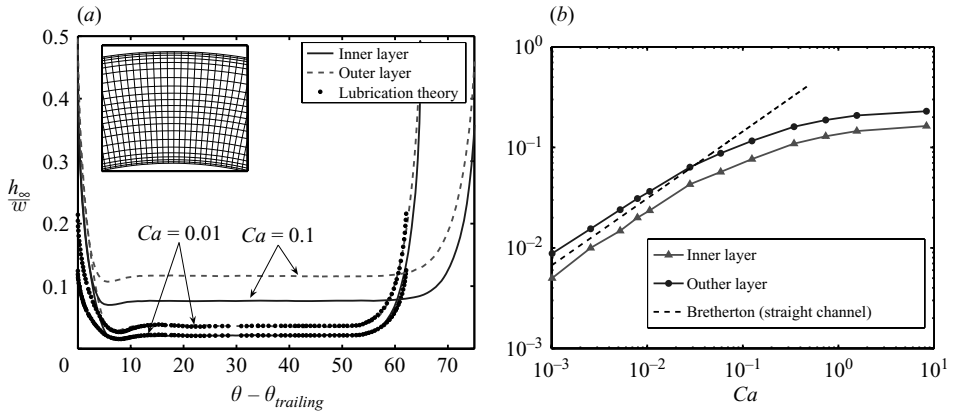

FIGURE 2. (*a*) Variation of inner and outer film thickness as a function of the arc angle measured from the trailing edge of the bubble for $Ca = 0.01$ and $Ca = 0.1$. The symbols indicate the film profiles obtained from the lubrication theory for $Ca = 0.01$ by Ratulowski & Chang (1989). The inset shows a portion of a typical (coarse) curvilinear grid containing 220×22 grid cells. (*b*) Inner and outer film thickness as a function of the capillary number. ($w/R_i = 0.333$, Grid : 640×64.)

to facilitate direct comparison with the lubrication theory. Note that the effects of Reynolds number are negligible when $Re < 10$ as discussed by Aussillous & Quere (2000).

First, the effects of the capillary number on the inner and outer layer film thickness are examined. The computations are performed using a semi-circular channel shown in figure 1(*a*) with the geometric parameter $w/R_i = 0.333$ and capillary numbers $0.001 \leqslant Ca \leqslant 8.325$. The film thickness of the inner and outer layers is plotted in figure 2(*a*) for $Ca = 0.1$ and $Ca = 0.01$ as a function of the arc angle measured from the trailing edge of the bubble to qualitatively demonstrate the influence of the capillary number and the difference between the film thickness of the inner and outer layers. The film profiles obtained from the lubrication theory by Ratulowski & Chang (1989) are also plotted for $Ca = 0.01$ in figure 2(*a*), scaled such that they correspond to the solution to (2.9) for inner and outer layers. As can be seen, the present computational results are in good agreement with the lubrication solution in most regions including the monotonic front and the undulating back profiles, but deviate at the trailing edge of the drop especially in the region away from the channel walls where the lubrication theory is not valid. We observe that the film is thinner in the inner layer than the outer layer and both film thicknesses grow with increasing capillary number as predicted by the lubrication theory. These observations are quantified in figure 2(*b*) where the film thickness of the inner and outer layers normalized by the channel width is plotted as a function of Ca; the dashed line shows the lubrication theory results for a corresponding straight channel (Bretherton 1961). The inner liquid layer is thinner while the outer layer is thicker than that of the corresponding straight channel.

The above numerical and analytical results are replotted in figure 3(*a*) by scaling the film thicknesses by the effective radii defined by equations (2.11) and (2.13), and using as the independent variable the effective capillary numbers defined by equations (2.7) and (2.13). Note that the effective radius and effective capillary number are different for the inner and outer layers. In figure 3(*a*), the dotted line indicates the

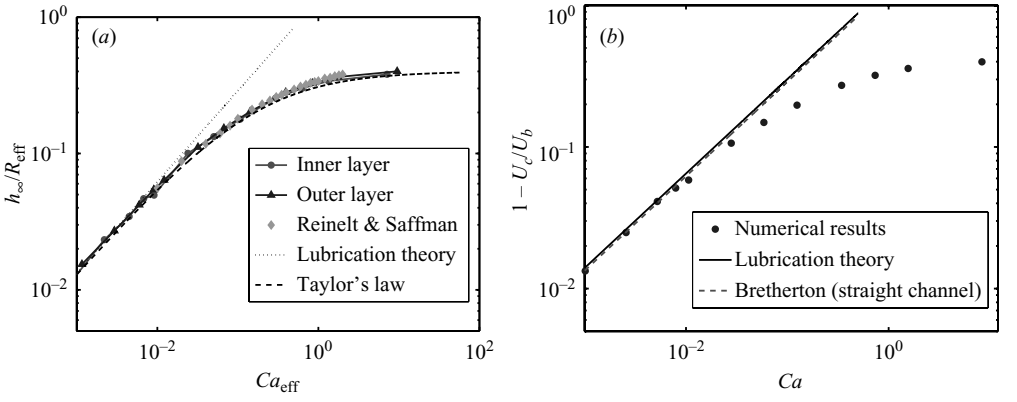

FIGURE 3. (*a*) The film thickness scaled by the effective radius versus the effective capillary number. The dashed line indicates the approximation $h_\infty/R_{\rm eff} = 1.34Ca_{\rm eff}^{2/3}/(1 + 1.34 \times 2.5Ca_{\rm eff}^{2/3})$. (*b*) The relative bubble velocity versus the capillary number. ($Ca = 0.01$ and $w/R_i = 0.333$.)

results of the lubrication theory and we also show as diamonds the computational results of Reinelt & Saffman (1985). The dashed line indicates the approximation

$$\frac{h_\infty}{R_{\rm eff}} = \frac{1.34Ca_{\rm eff}^{2/3}}{1 + 1.34 \times 2.5Ca_{\rm eff}^{2/3}}, \tag{3.1}$$

which has been shown to fit the available experimental data very well for the straight channel case (Aussillous & Quere 2000). It can be seen that the scaled inner and outer film thicknesses approximately collapse onto the same curve and the computational results match well with the lubrication theory for $Ca_{\rm eff} \leqslant 0.01$. There is a significant difference between the numerical and lubrication results for larger effective capillary numbers. The numerical results are also in a good agreement both with the finite-difference solutions of Reinelt & Saffman (1985) and the approximation (3.1).

The lubrication theory predicts that the bubble moves faster than the average velocity of the flow in the channel. This result is verified in figure 3(*b*) where the numerical results are plotted together with the lubrication theory. As can be seen, the numerical results match well with the lubrication theory for small capillary numbers, i.e. $Ca < 0.01$, but deviate significantly for larger capillary numbers. It is also seen that the bubble velocity is slightly larger in the curved channel than in the corresponding straight channel ($w/R_i = 0$).

The effects of the channel curvature on the film thicknesses are examined next. For this purpose, the numerical computations are performed for various values of channel curvature while keeping the capillary number constant at $Ca = 0.01$. Figure 4(*a*) shows the non-dimensional film thickness (h_∞/w) of the inner and outer layers as a function of the non-dimensional channel curvature (w/R_i). The symbols indicate the numerical results while the solid lines are the results of the lubrication theory. The ratio of the outer film thickness to the inner film thickness is also plotted as an inset. It can be observed that the inner film thickness decreases whereas the outer film thickness increases with increasing channel curvature as predicted by the lubrication theory. It is also observed that the numerical results are overall in good agreement with the lubrication theory. The differences between the computational results and

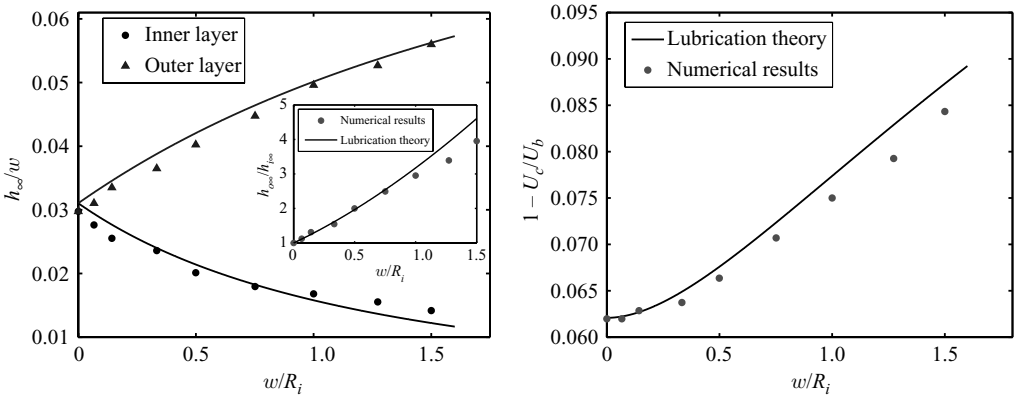

FIGURE 4. (*a*) Variation of film thickness in the inner and outer layers as a function of the non-dimensional channel curvature. The inset shows the ratio of the outer film thickness to the inner film thickness. (*b*) The relative bubble velocity versus the non-dimensional channel curvature. $Ca = 0.01$.

the lubrication theory are partly attributed to the finite value of the capillary number, i.e. $Ca = 0.01$.

Finally, the bubble velocity relative to the average flow velocity in the channel is plotted in figure 4(*b*) as a function of the non-dimensional channel curvature. The results show good agreement between the computational results and the lubrication theory for small channel curvatures.

4. Bubble in a curved tube with circular cross-section

We now consider the analogous situation of a bubble translating along a curved channel of circular cross-section. Again, we work with the 'Bretherton' limit where the bubble is long compared to the tube radius (a). Denoting the centreline radius as R_c, the surface of the torus is then given in terms of the angular variables ψ and ϕ by

$$x = (R_c + a\cos\psi)\cos\phi, \quad y = (R_c + a\cos\psi)\sin\phi, \quad z = a\sin\psi, \tag{4.1}$$

where the origin for the Cartesian coordinates (x, y, z) is located at the centre of the circular channel. Now consider a differential strip on the torus aligned with the bubble with $a\mathrm{d}\psi$ being the arclength of the strip. We denote the film thickness on this element as $h(\phi, \psi)$. In the low-capillary-number limit the variation with ψ occurs on the scale a, while we expect the thin film to also vary slowly with ϕ except in a narrow transition region $O(aCa_{\mathrm{eff}}^{2/3})$, where Ca_{eff} is an appropriately defined capillary number given below. Thus a lubrication approach is appropriate and the mean curvature of the interface can be approximated as

$$\kappa \cong \frac{1}{a} + \frac{\cos\psi}{r^*} + \frac{1}{r^{*2}}\frac{\partial^2 h}{\partial\phi^2}, \tag{4.2}$$

where $r^* = R_c + a\cos\psi$. When the bubble moves at a steady velocity U_b, then the film thickness is given by

$$\frac{u_s(\psi)(h - h_\infty(\psi))}{h^3} = \frac{\sigma}{3\mu r^{*3}}\frac{\partial^3 h}{\partial\phi^3}, \tag{4.3}$$

where the surface velocity is defined as $u_s = (1 + (a/R_c)\cos\psi)U_b$. This equation is simply a local version of the LLDB result where the film profile $h(\phi, \psi)$ has the ψ variations slaved to the variation of surface speed $u_s(\psi)$. The boundary conditions are $h \to h_\infty$, $\partial h/\partial\phi \to 0$ and $\partial^2 h/\partial\phi^2 \to 0$ in the inner film region while the curvature approaches the mean curvature of a sphere of radius a, i.e.

$$\frac{1}{r^{*2}}\frac{\partial^2 h}{\partial\phi^2} \to \frac{1}{a} - \frac{\cos\psi}{R_c + a\cos\psi}$$

in the outer film region. We denote the ϕ-independent film thickness near the centre of the bubble as $h_\infty(\psi)$, and the effective capillary number as $Ca_{\text{eff}} = \mu u_s(\psi)/\sigma$. Then analogous to the characterization of the two-dimensional problem, let

$$\eta = h/h_\infty(\psi) \text{ and } \xi = \frac{r * \phi}{h_\infty(\psi)}(3Ca_{\text{eff}})^{1/3},$$

which earlier led to equation (2.9). Using the boundary conditions, the ψ-dependent film thickness is now given by

$$h_\infty(\psi) = 1.3375R_{\text{eff}}(Ca_{\text{eff}})^{2/3}, \tag{4.4}$$

where

$$R_{\text{eff}} = a\left(1 + \frac{a}{R_c}\cos\psi\right). \tag{4.5}$$

From conservation of mass, the bubble velocity relative to the average liquid velocity is given by

$$\frac{U_b - U_c}{U_b} = c_2\left(1.3375Ca^{2/3}\right) \tag{4.6}$$

where the coefficient c_2 is given by the integral

$$c_2 = \left[\frac{1}{\pi}\int_0^{2\pi}\left(1 + \frac{a}{R_c}\cos\psi\right)^{8/3}\mathrm{d}\psi\right] \cong 2 + \frac{20}{9}\left(\frac{a}{R_c}\right)^2 - \frac{5}{162}\left(\frac{a}{R_c}\right)^4 + O\left(\frac{a}{R_c}\right)^6; \tag{4.7}$$

we have given the first three terms in an expansion in powers of $(a/R_c)^2$, since this is likely to cover most conditions of interest. Note that $c_2 = 2$ corresponds to a straight channel (Bretherton 1961). Equations (4.6) and (4.7) show that the bubble again moves faster in a curved circular channel than in a corresponding straight channel and that the bubble velocity increases monotonically with the channel curvature as in the two-dimensional case.

5. Conclusions

The motion of large bubbles in uniformly curved channels has been studied both theoretically using the lubrication approximation and computationally using a finite-volume/front-tracking method. In the low-capillary-number limit, we show that the steady film thickness is governed by the classical Landau–Levich–Dejaguin–Bretherton (LLDB) equation but the boundary conditions are modified to account for the channel curvature. The film in the outer layer is thicker than in the inner layer, the difference between film thicknesses increases monotonically as the channel curvature increases, and scaling rules relating the film thicknesses to the channel curvature, the capillary number and channel width are given. The results also show that the bubble velocity, relative to mean liquid speed, is always larger than that in a

corresponding straight channel and increases monotonically with increasing channel curvature. Extensive numerical simulations are performed for two-dimensional cases and show good agreement with the lubrication predictions for small capillary numbers, i.e. $Ca \leqslant 0.01$, and for small or moderate channel curvatures, i.e. $w/R_i \leqslant 0.75$. The computational results are in good agreement with the finite-difference solutions for a bubble in a straight channel obtained by Reinelt & Saffman (1985) for a wide range of capillary numbers when the quantities are rescaled as suggested by the lubrication analysis. Finally, we developed a lubrication approach for the motion of large bubbles in a curved channel of circular cross-section.

We thank the Harvard MRSEC (DMR-0213805) and Unilever Research for partial support of this research. The first author (M.M.) is partially supported by the Scientific and Technical Research Council of Turkey (TUBITAK). We thank P. Garstecki, A. Guenther, M. Kreutzer, and M. de Menech for helpful conversations.

REFERENCES

Aussillous, P. & Quere, D. 2000 Quick deposition of a fluid on the wall of a tube. *Phys. Fluids* **12**, 2367–2371.

Bretherton, F. P. 1961 The motion of long bubbles in tubes. *J. Fluid Mech.* **10**, 166–188.

Garstecki, P., Fischbach, M. A. & Whitesides, G. M. 2005 Design for mixing using bubbles in branched microfluidic channels. *Appl. Phys. Lett.* **86**, 244108.

Gaver, D. P., Halpern, D., Jensen, O. E. & Grotberg, J. B. 1996 The steady motion of a semi-infinite bubble through a flexible-walled channel. *J. Fluid Mech.* **319**, 25–65.

Guenther, A., Jhunjhunwala, M., Thalmann, M., Schmidt, M. A. & Jensen, K. F. 2005 Micromixing of miscible liquids in segmented gas-liquid flow. *Langmuir* **21**, 1547–1555.

Guenther, A., Khan, S. A., Trachsel, F., Thalmann, M. & Jensen, K. F. 2004 Transport and reaction in microscale segmented flow. *Lab on a Chip* **4**, 278–286.

Halpern, D. & Jensen, O. E. 2002 A semi-infinite bubble advancing into a planar tapered channel. *Phys. Fluids* **14**, 431–442.

Howell, P. D. 2003 Surface-tension-driven flow over a moving curved surface. *J. Engng Maths* **45**, 283–308.

Landau, L. & Levich, B. 1942 Dragging of liquid by a plate. *Acta Physiochim. USSR* **17**, 42–54.

Mazouchi, A. & Homsy, G. M. 2001 Free surface stokes flow over topography. *Phys. Fluids* **13**, 2751–2761.

Muradoglu, M. & Gokaltun, S. 2004 Implicit multigrid computations of buoyant drops through sinusoidal constrictions. *Trans. ASME J. Appl. Mech.* **71**, 857–865.

Muradoglu, M. & Kayaalp, A. 2006 An auxiliary grid method for computations of multiphase flows in complex geometries. *J. Comput. Phys.* **214**, 858–877.

Muradoglu, M. & Stone, H. A. 2005 Mixing in a drop moving through a serpentine channel: A computational study. *Phys. Fluids* **17**, 073305.

Quere, D. 1999 Fluid coating on a fiber. *Annu. Rev. Fluid Mech.* **31**, 347–384.

Ratulowski, J. & Chang, H.-C. 1989 Transport of gas bubbles in capillaries. *Phys. Fluids* A **1**, 1642–1655.

Reinelt, D. A. 1995 The primary and inverse instabilities of directional viscous fingering. *J. Fluid Mech.* **285**, 303–327.

Reinelt, D. A. & Saffman, P. G. 1985 The penetration of a finger into a viscous fluid in a channel and tube. *SIAM J. Sci. Statist. Comput.* **6**, 542–557.

Roy, R. V., Roberts, A. J. & Simpson, M. E. 2002 A lubrication model of coating flows over a curved substrate in space. *J. Fluid Mech.* **454**, 235–261.

Schwartz, L. W. & Weidner, D. E. 1995 Modeling of coating flows on curved surfaces. *J. Engng. Maths* **29**, 91–103.

Song, H., Bringer, M. R., Tice, J. J., Gerdts, C. J. & Ismagilov, R. F. 2003 Scaling of mixing by chaotic advection in droplets moving through microfluidic channels. *Appl. Phys. Lett.* **83**, 4662–4666.

Squires, T. M. & Quake, S. R. 2005 Microfluidics: Fluid physics at the nanoliter scale. *Rev. Mod. Phys.* **77**, 977–1026.

Stone, H. A., Stroock, A. D. & Ajdari, A. 2004 Engineering flows in small devices: Microfluidics toward a lab-on-a-chip. *Annu. Rev. Fluid Mech.* **36**, 381–411.

Stone, Z. B. & Stone, H. A. 2005 Imaging and quantifying mixing in a model droplet micromixer. *Phys. Fluids* **17**, 063103.

Thulasidas, T. C., Abraham, M. A. & Cerro, R. L. 1995 Bubble-train flow in capillaries of circular and square cross section. *Chem. Engng Sci.* **50**, 183–199.

Tryggvason, G., Bunner, B., Esmaeeli, A., Juric, D., Al-Rawahi, N., Tauber, W., Han, J., Nas, S. & Jan, Y.-J. 2001 A front-tracking method for the computations of multiphase flow. *J. Comput. Phys.* **169**, 708–759.

Unverdi, S. & Tryggvason, G. 1992 A front-tracking method for viscous, incompressible multi-fluid flows. *J. Comput. Phys.* **100**, 25–37.

Wong, H., Radke, C. J. & Morris, S. 1995 The motion of long bubbles in polygonal capillaries. Part 1. Thin films. *J. Fluid Mech.* **292**, 71–94.